Scanning Ion Microscopy with Low Energy Lithium Ions

Kevin A. Twedt,[1, 2] Lei Chen,[1] and Jabez J. McClelland[1]

[1] Center for Nanoscale Science and Technology, National Institute of Standards and Technology, Gaithersburg, MD 20899, USA
[2] Maryland NanoCenter, University of Maryland, College Park, MD 20742, USA

Abstract

Using an ion source based on photoionization of laser-cooled lithium atoms, we have developed a scanning ion microscope with probe sizes of a few tens of nanometers and beam energies from 500 eV to 5 keV. These beam energies are much lower than the typical operating energies of the helium ion microscope or gallium focused ion beam systems. We demonstrate how low energy can be advantageous in ion microscopy when detecting backscattered ions, due to a decreased interaction volume and the potential for surface sensitive composition analysis. As an example application that demonstrates these advantages, we non-destructively image the removal of a thin residual resist layer during plasma etching in a nano-imprint lithography process.

1. INTRODUCTION

Charged particle sources from laser-cooled atomic gases are showing increasing promise as new tools in nanoscale science and technology. The extremely low temperatures achievable with laser cooling, routinely in the microkelvin range, have made possible a new generation of focused ion beam (FIB) sources with high brightness, low energy spread, and a choice of over 20 different ionic species [1]. Several sources have already been developed, including a pulsed rubidium ion source [2,3] and complete FIB systems for chromium [1,4] and lithium [5]. An improved source design using a cold atomic beam of cesium was recently realized [6], with measurements indicating a brightness and energy spread superior to that of the widely used gallium liquid metal ion source (LMIS). Cold atoms are also being used to produce electron sources with a unique combination of high coherence and high brightness [7–9], and the potential to improve ultrafast electron diffraction imaging of molecular structure dynamics. This promising set of tools is likely to provide improvements to all of the standard ion and electron beam applications in high-resolution imaging, nanomachining, material deposition, and sample composition analysis.

In this paper, we report on a cold atom based lithium FIB configured as a low energy scanning ion microscope. Scanning ion microscopy offers good surface sensitivity and distinct contrast mechanisms compared to scanning electron microscopy (SEM), as has been shown with the standard gallium FIB [10] and the helium ion microscope (HIM) [11]. Like helium, the low mass of lithium makes it ideal for imaging applications where sample sputtering must be minimized. Unlike the HIM, our lithium ion source is well suited for operation at low beam energies in the range of a few thousand electron volts or even less.

Low energy is advantageous in ion microscopy when imaging with backscattered ions, as the interaction volume is reduced and the backscatter yield is increased. In addition, low energy ions can be used to probe the composition and structure of surfaces with high sensitivity to the topmost layers. This sensitivity has been exploited in the well-established field of low energy ion scattering (LEIS), or ion scattering spectroscopy (ISS) [12–14]. Typical LEIS instruments are limited to relatively large probe sizes of millimeter scale, however, and are generally not used in an imaging mode. Our system has demonstrated a probe size less than 100 nm for beam energies as low as 700 eV, and our best achieved resolution thus far is 27 nm at a beam energy of 2 keV and a beam current of 1 pA [5]. At these low energies, no other FIB system has demonstrated this level of performance.

In the following sections, we review the design of the lithium FIB and show the imaging modes of the microscope. We discuss the influence of beam energy on the imaging modes and explore advantages to using a low energy beam. We also discuss the possibility of combining high resolution ion microscopy with surface-sensitive composition analysis similar to LEIS. As a demonstration of the advantage of low energy ion imaging, we image the removal of a thin residual resist layer during a plasma etching step in a nano-imprint lithography (NIL) process.

2. THE LITHIUM ION MICROSCOPE

2.1. Instrument design

The design and performance of the lithium FIB has been presented previously [5], and we will summarize the results here. A good general review of cold atom ion sources can be found in

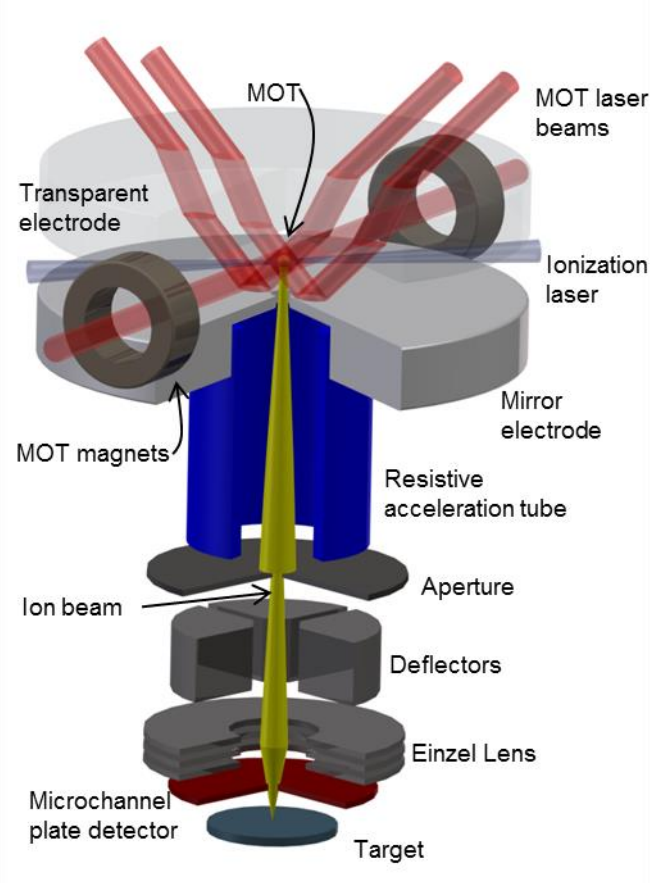

Figure 1. Schematic of the lithium ion microscope.

the introduction of reference [15]. Neutral lithium atoms are laser-cooled and trapped in a magneto-optical trap (MOT) at a temperature of about 600 μK. The MOT is created between two electrodes as shown in the schematic in Fig. 1. The atoms are photoionized in an electric field by an additional laser, and the ions are accelerated through a hole in the bottom electrode.

A resistive tube accelerator is used to accelerate the ions to the final beam energy, while keeping a low electric field over the region of ionization, reducing the energy spread of the beam to less than 100 meV. The small electric field at the source and the low energy spread make the source ideal for operation at low energies. Achievable beam energies are currently in the range of 500 eV to 5 keV. Although the beam energy can be set arbitrarily low with this design, repulsive Coulomb interaction effects at the source limit the achievable spot size when the accelerating field is too low [16].

After exiting the resistive tube, the ions are coupled into an electrostatic ion optical column that is part of a commercial FIB system. The beam is aligned through the column, corrected for astigmatism, and focused onto a sample stage. Images are created by scanning the beam across the sample and collecting secondary electrons or backscattered ions. The beam resolution of this system has been measured at various energies by imaging while scanning across a knife edge [5]. At a beam energy of 2 keV the source demonstrated a focal spot of 27 nm at a current of 1 pA. Based on this measurement, we estimate the brightness of the ion beam to be 0.6×10^4 A m^{-2} sr^{-1} eV^{-1}, but this is by no means a fundamental limit. We estimate that reasonable increases to the cold atom flux and ionization rate could improve the source

brightness by one to two orders of magnitude.

A custom annular microchannel plate (MCP) detector is mounted at the base of the ion optical column. A bias voltage applied to the front of the MCP, relative to the grounded sample stage, enables efficient detection of either secondary electrons or backscattered lithium ions. The MCP assembly is only 3 mm thick, which allows for the short working distances necessary to achieve the highest resolution images. The fields generated by the voltages on the MCP have a minimal impact on the ion beam parameters.

2.2. Imaging modes

We will now review the imaging modes of a scanning ion microscope and show example lithium ion images. Ion imaging modes have been studied extensively for the gallium FIB [10,17] and the HIM [18–21], and a lithium microscope is expected to behave in essentially the same way. When ions enter the target, ion-induced secondary electrons (iSE) are generated along the ion trajectory, and those generated near the surface can escape. As the ions travel through the target, they lose energy through inelastic interaction with the electron fluid (electronic stopping) and through elastic collisions with the target nuclei (nuclear stopping). A single or a series of elastic collisions can result in the incident ion being scattered back out of the sample as a backscattered ion (BSI). Images can be created by scanning the primary beam across the surface of the target and collecting either iSEs or BSIs. Under some circumstances, BSIs can become neutralized during the scattering process, and leave the surface as energetic neutral atoms. Also, ions or neutrals from the target can be ejected (sputtered) with varying degree of likelihood. In principle, the backscattered neutrals and sputtered ions could also be collected, but for a lithium ion beam in our energy range the rates of these two processes are low.

Imaging with iSE in an ion microscope has some differences and advantages when compared to imaging with electron-induced secondary electrons (eSE) in a SEM. A primary advantage is the increased surface sensitivity due to the high percentage of iSEs that come from the ion beam entrance point. The total iSE signal includes the iSEs generated when the primary beam enters the target (generally called iSE-1), those generated by the BSIs when they exit the surface (iSE-2), and those generated by the BSIs when they strike a different surface in the vacuum chamber (iSE-3). Since the BSIs (or backscattered electrons in an SEM) exit the target over a spatial region typically much larger than the beam focal spot, a large SE-2 or SE-3 signal can reduce the resolution and surface sensitivity of the image. For the HIM, it has been found that the SE-1/SE-2 ratio is typically higher than that for SEM. This is especially true at high beam energies (>30 keV), as the iSE yield increases and the BSI yield decreases. But simulations suggest it may also be true at lower energies (down to at least 5 keV), depending on the composition of the surface [19]. We expect that iSE imaging with lithium ions in these same energy ranges will provide the same advantage as helium.

Another primary difference in SE imaging between ion and electron microscopes is the charge contrast generated on partially insulating samples. If a surface is completely insulating and has no charge dissipation, then the ion induced charging will eventually become great enough to affect the incoming beam and imaging will not be possible. However, there is a wide range of samples and scan rates where charging is mild enough to trap iSEs but not strong enough to appreciably influence the incident beam. On these samples the insulating region charges positively under the ion beam, creating a local field that traps the low energy iSE at the surface, rendering the region dark. The result can be a stark contrast between the insulating and

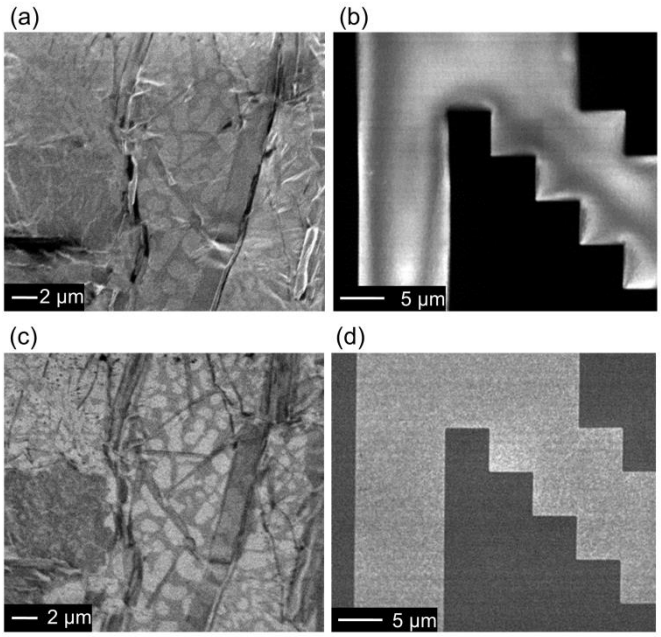

Figure 2. Lithium ion microscope images. (a) Secondary electron and (c) backscattered ion images of a lead-tin solder dot. The iSE image is governed predominantly by topographic contrast, while the BSI image is dominated by atomic numbr contrast. (b) Secondary electron and (d) backscattered ion images of a metal on oxide test pattern. The charged oxide appears black in the iSE image and the charging causes distortions along the metal-oxide interface. The BSI image shows elemental contrast and has no adverse effects from the charging.

conducting regions. By comparison, in a SEM insulating surfaces will generally charge negatively, resulting in images that can be difficult to interpret, but can charge positively at low beam energy when the SE yield exceeds the primary beam current.

Examples of lithium iSE images are shown in Fig. 2[(a) and (b)]. Figure 2(a), an image of a lead-tin solder dot, appears to be a fairly conventional secondary electron image of a metal, showing contrast mainly influenced by topography. Fig. 2(b), which shows an image of a conducting metal pattern on an insulating oxide, illustrates the effects of charge contrast. In this image, the oxide is completely dark, while the metal is bright, with some shading resulting from charge distribution on its surface.

Examples of lithium BSI images are shown in Fig. 2[(c) and (d)]. The backscatter rate varies greatly with the atomic number of the atoms in the target, so the backscatter image of the lead-tin solder dot in Fig. 2(c) gives good elemental contrast. Interestingly, the metal-on-insulator image in Fig. 2(d) is apparently immune to the charging effects present in the iSE image. The ions backscatter from the surface with a significant fraction of the primary beam energy so they are less affected by charging on the surface compared to the very low energy (1 eV to 10 eV) secondary electrons.

3. ADVANTAGES OF LOW ENERGY

Ion microscopy, like electron microscopy, stands to benefit from access to a full range of beam energies. Existing instrumentation for scanning ion microscopy is limited to the gallium FIB and the HIM, which have typical operating energies of 2 to 30 keV and 10 to 40 keV respectively. While the brightness of our lithium source does not yet match either of these instruments, it performs comparably well at low beam energies. The gallium LMIS can be operated at low energy, but the beam resolution suffers due to chromatic aberrations arising from the relatively large (≈ 5 eV) energy spread of the source. The gas field ionization source (GFIS) used in the HIM has an ideal operating energy around 30 keV and the source current drops significantly as the energy is reduced [11]. The low energy operation of the HIM has not been well characterized, and we are not aware of any attempts to use it below 10 keV. Even if the helium GFIS cannot be easily operated at lower energies, it seems likely that a high resolution low energy beam could be produced by combining the 30 keV GFIS with an ion column designed to allow beam deceleration. In either case, a low energy helium FIB has not yet been demonstrated.

In this section, we will discuss how ion microscopy imaging modes depend on the energy of the primary ion beam. We will focus on backscatter imaging where low energy ions have an advantage. We also explore the use of low energy ions as a microanalysis tool to extract high resolution composition information about the surface. The results are applicable both to our lithium FIB and to any future helium FIB that may be configured for low energy.

3.1. Backscatter Yield and Interaction Volume

Scanning ion microscopy with iSEs is generally expected to improve with increasing beam energy. First of all, the focal spot size achieved by the ion beam generally shrinks with increasing energy. Also, the yield of iSEs increases with energy, not peaking until well over 100 keV [19]. Furthermore, as mentioned previously, the SE-1/SE-2 ratio improves with increasing energy, resulting in a smaller effective probe size and greater surface sensitivity.

On the other hand, imaging with backscattered ions should improve with decreasing beam energy, both in the effective probe size and the backscatter yield. The backscatter yield is related to the standard Rutherford scattering cross section,

$$\sigma \propto (Z_1 Z_2 / E)^2,$$

which increases with the atomic number of the incident ion, Z_1, and target ion, Z_2, and increases for lower beam energy, E. As the beam energy increases, nuclear scattering is less frequent and more energy is lost through electronic stopping, resulting in fewer ions being backscattered from the sample. To elucidate this energy and atomic number dependence, we used SRIM simulations [22] to calculate the fraction of backscattered ions for a lithium beam of varied energy at normal incidence onto pure targets of carbon, silicon, copper, and gold. The results are shown in Fig. 3. These calculations show that while low energy improves the backscatter yield for all target elements, it is particularly advantageous for low atomic number targets.

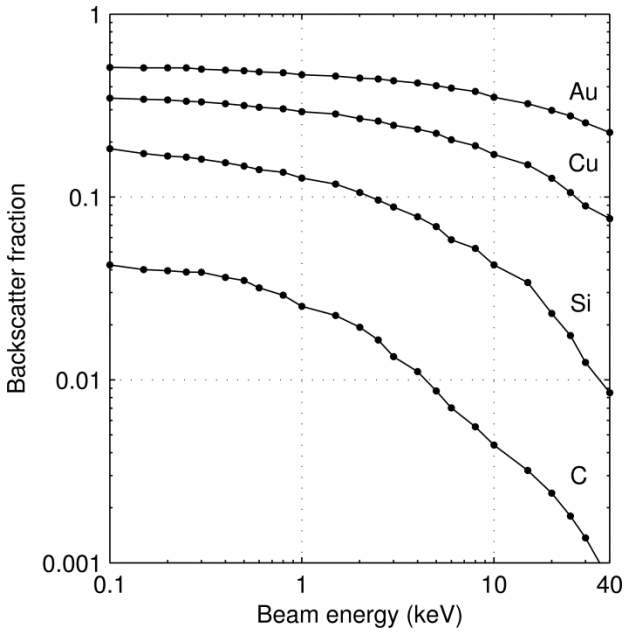

Figure 3. SRIM calculated backscattered ion yield for lithium ions incident on targets of carbon, silicon, copper, and gold. Each point is the result of 40 000 incident ion trajectories.

To illustrate the effect on probe size, we used SRIM to track the paths of ions as they move through the target. Figure 4 shows trajectories of 30 keV and 2 keV lithium ions entering a silicon target. Only the trajectories of ions that get backscattered from the target are displayed, as these are the ions that contribute to the BSI image. It is clear that the 2 keV ions have a much smaller interaction volume than the 30 keV ions, and hence should have a better image resolution.

The effect on imaging resolution of course depends greatly on the type of elements and features within the sample. For example, Fig. 4 suggests that the lateral resolution of a 30 keV BSI image would be nearly 100 nm even for a sharp beam focus. But for 30 keV HIM imaging of some common samples the resolution has been found to be closer to 10 nm [18], and can be even better for favorable imaging targets [23] (note that helium ions have a slightly larger range than lithium ions of the same energy).

In addition to reducing lateral resolution, the depth of the BSI trajectories can result in sub-surface blurring of the images. Ion beams at 30 keV can easily pass through surface layers up to 50 nm in thickness and the BSI signal will include ions that have scattered off both the surface layer and the underlying layer, potentially degrading the elemental contrast. In the next section, we explicitly demonstrate the surface sensitivity of low energy BSIs by imaging a thin resist film on a silicon substrate.

3.2. Surface Composition Analysis

We now consider the possibility of using the backscattered ion signal to do composition analysis of surfaces. For the purposes of qualitative imaging, sufficient information can often be obtained from the variation in signal yield on different surfaces, so we will examine this first.

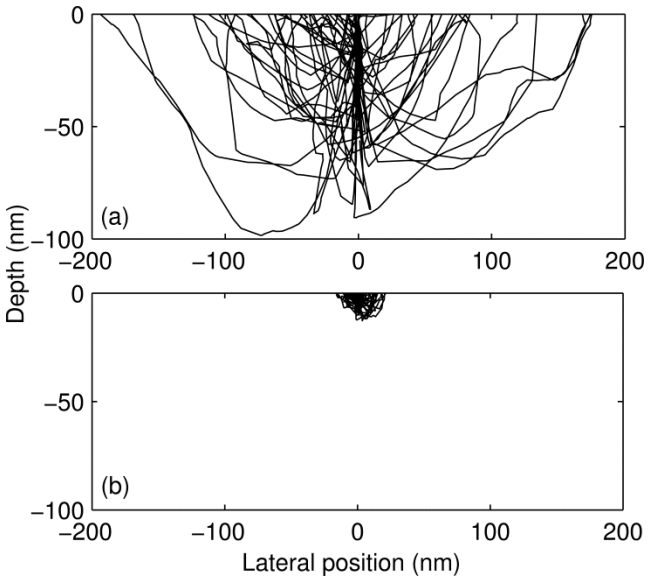

Figure 4. Trajectories of (a) 30 kV and (b) 2 kV lithium ions backscattered from a silicon target. Each plot has trajectories for 70 backscattered ions, but the fraction of total ions that are backscattered is only 1.2 % for 30 kV compared to 11 % for 2 kV.

To explore the dependence on atomic number, we have measured the backscatter yield of 4 keV Li ions from a set of 16 pure elemental samples covering a wide range of atomic numbers. The results are plotted and compared to SRIM simulations in Fig. 5. We find that the yield generally increases with atomic number and can be nearly as high as 50 % for high atomic number targets. We note that these data were taken for an ion beam at normal incidence to the sample; the yield will only increase for scattering at an angle.

The target consisted of commercially available element standards in the form of 3 mm diameter discs held in a stainless steel retainer. We acquired a low magnification BSI image of each disc and determined the backscatter yield of each element standard relative to the stainless steel frame by comparing the average gray levels in each image. The average gray level was calculated over nearly the entire area of the disc (avoiding only the outer edges where it contacts the retainer). In order to estimate the uncertainty in gray level, the images were first sent through a 20 μm radius median filter, which removes the Poisson noise associated with the low beam current, and then the standard deviation over the area of the disc was calculated. This uncertainty, indicated by error bars in Fig. 5, represents the random mesoscopic variations in signal over the area of each element standard.

To put the backscatter yields on an absolute scale, we measured the absolute backscatter fraction for the gold sample and scaled all gray level measurements relative to the gold measurement. The gold backscatter yield was measured to be 0.44 ± 0.07 by comparing the ion current on the sample stage to the actual beam current. During this measurement, the MCP was biased at -1000 V relative to the stage, to ensure that all backscattered ions and no secondary electrons leave the sample. The sample current in this case could be considered to be equal to the beam current minus the backscatter current, as long as sputtered ions and/or primary or sputtered neutrals can be ignored. We note that this scaling introduces an absolute scale factor uncertainty of ±16 % for all the measurements shown in Fig. 5.

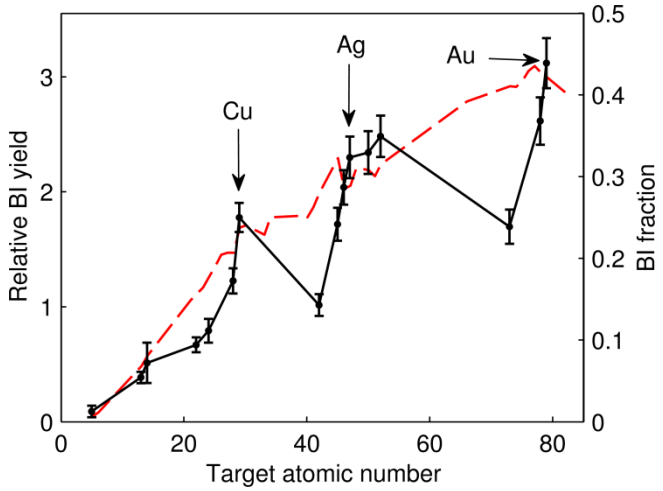

Figure 5. Fraction of 4 keV lithium ions backscattered from pure elemental targets. The black solid line is the measured backscatter yield of each target relative to the backscatter yield of the stainless steel retainer (left vertical axis). The red dashed line is the fraction of ions backscattered from the target calculated using SRIM (right vertical axis). To compare the data and simulations, the two vertical axes are aligned based on an absolute backscatter fraction measurement on the gold target of 0.44 ± 0.07. Arrows indicate the data points for copper, silver, and gold, which share a column of the periodic table. All uncertainties are a single standard deviation combined standard uncertainty.

The oscillations in the yield with atomic number seen in Fig. 5 are not predicted by the SRIM simulations, and may be the result of two complicating factors. First, there is generally a surface oxide layer on many of the element standards, which were polished and mounted in air before being loaded into the high vacuum environment. At low energy, the range of the ion beam may not be enough to penetrate the oxide and the yield from metal samples will be reduced by the lower scattering rate from the oxygen atoms. However, in an attempt to avoid this problem we have chosen a set of elements that are known to not form thick oxide layers. As evidence that this is not a significant issue in our case, we have made the same measurement with a 1 keV lithium beam (which should be much more sensitive to surface layers) and we observe oscillations at the same values of atomic number and with nearly the same amplitude.

Second, a theoretical analysis suggests that oscillations in the electronic stopping power with atomic number occur when effects not taken into account by the SRIM calculation are included [24]. This is supported by the fact that similar oscillations were observed in backscatter yield measurements in the HIM [25], and these measurements are even less likely to have been affected by an oxide layer due to the higher beam energy and larger interaction volume. Although at 4 keV the electronic stopping power is much less than it is at 30 keV, and is comparable to the nuclear stopping power, these effects may still be significant enough to cause the oscillations seen in our data.

In either case, these measurements show that good contrast can be expected in backscattered ion images with varying composition, but variations in the backscatter yield alone are not likely to provide unambiguous elemental identification on a sample. Also, even if the backscatter rate were a single-valued function of atomic number, rate measurements alone would

not be able to accurately identify areas of a sample where multiple elements are present.

Quantitative composition analysis with ion beams can be done by detecting the energy spectrum of the backscattered ions. In a single scattering event, the energy of the scattered ion is given by [14]

$$E = E_0 \left(\frac{\cos\theta \pm \sqrt{(m_2/m_1)^2 - \sin^2\theta}}{1 + m_2/m_1} \right)^2$$

where E_0 is the energy of the incident ion, m_1 the mass of the incident ion, m_2 the mass of the target atom, and θ the scattering angle. By measuring the energy of scattered ions collected in a narrow angular spread, the mass of the target atoms can be determined. This simple principle has long been used to determine the composition of surfaces in LEIS experiments. The experiments typically use noble gas or alkali atoms of 100 eV to 10 keV energies scattered at an angle off a surface. Detectors such as electrostatic or time-of-flight energy analyzers record the energy spectrum of the ions scattered at a specific angle and the peaks in the energy spectrum indicate the atomic masses in the target. The low penetration depth of low energy ions makes this technique very surface sensitive and is typically used in applications in catalysis and thin film metrology [13]. But LEIS instruments to date have been limited to low brightness sources and large area analysis. By implementing an energy analyzer in a low energy ion microscope, we could in principle achieve all of the same goals, but with much higher spatial resolution. We note that elemental analysis, including some energy spectra, has been studied with the HIM [21,25,26], but the lack of surface sensitivity from the high energy beam is evident.

3.3. Composition Analysis with Lithium

Thus far, we have described the properties of ion microscopy as being mostly independent of the ion used, except for the increased sputtering damage caused by the heavier gallium ions. But especially when considering composition analysis with low energy ion scattering, the choice of ion can make a significant difference. Scattering of light ions like lithium and helium is ideal for differentiating light elements within a sample, but not for differentiating heavy elements. This can be easily seen by considering the scaling of the scattered ion energy. At $\theta = 180°$, $E = E_0[1 - 2m_1/(m_2 + m_1)]$. When $m_1 \ll m_2$, the energy is close to the incident ion energy and small changes in the target mass are hard to resolve. Thus in ion scattering measurements, it is best to use light ions for light targets and heavy ions for heavy targets (if the additional sputtering of the heavy ion can be tolerated). We note that all of the stable alkalis and noble gases have been successfully laser-cooled, and a high-brightness low-energy ion source with performance comparable to our lithium source could in principle be created with any of these elements.

Given that a low energy ion microscope could be realized for either helium or lithium, it is further instructive to consider the relative advantages of the two elements. There is a significant difference in ion-surface interactions for lithium ions compared to helium ions [14]. Low energy noble gas ions have a high probability of neutralizing in the sample. For certain targets, the neutralization of helium is so efficient that the ion backscatter yield can be two orders of magnitude lower than for lithium at the same energy [27]. The neutralization probability generally increases as the beam energy is lowered [28]. This neutralization is often exploited to make noble gas LEIS instruments uniquely sensitive to the topmost atomic layer of a surface, as

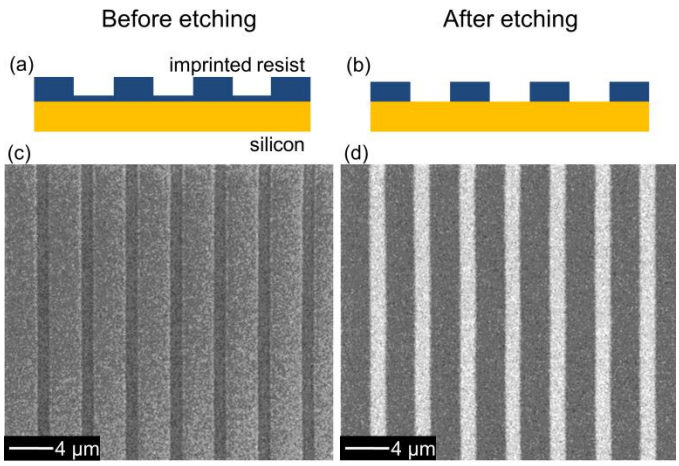

Figure 6. Backscattered lithium ion images of a NIL grating. (a)-(b) Schematic of imprint and etching process. (c)-(d) Images before and after oxygen plasma etching. The images were taken using the same beam parameters (2 kV, 1 pA) and detector settings, and have been processed identically.

ions that travel past the top layer are much more likely to neutralize in the sample. Alkali LEIS lacks the extreme surface sensitivity, but has the advantage in signal strength.

For high resolution imaging, the dose of ions used is of critical importance. The detection system will set a limit on the number of ions that need to be scattered to complete a measurement. The volume of the sample that is sputtered by this ion dose will limit the best achievable resolution of the LEIS technique, with a potential tradeoff between surface sensitivity and lateral resolution. We note that, very recently, an inductively coupled plasma helium ion source has been added to the LEIS instrument of reference [13] and LEIS data have been recorded with a lateral resolution of 5 μm [29]. At this resolution the technique can still be sensitive to the topmost atomic layer, but at higher resolution the surface sensitivity will be determined by the sputtering depth. For LEIS with sub-micrometer resolution, the higher backscatter yield of lithium could be a significant advantage, despite having a slightly higher sputtering rate than helium.

4. NANO-IMPRINT LITHOGRAPHY

Leaving quantitative energy analysis to future implementations of our Li ion microscope, we focus on imaging applications where contrast in backscatter yield can be used to identify sample composition. Based on the results of the previous section, our technique is ideal for imaging thin films with elemental contrast at a 10 nm depth level. It is also well suited for detecting light elements: the slope of the backscatter yield curve, both as a function of beam energy and atomic number, is steeper at lower atomic numbers. As an example of the utility of this approach, we examined a thermoplastic resist patterned by NIL. The goal is to non-destructively detect the presence or absence of a thin residual layer of the organic resist on top of a silicon substrate.

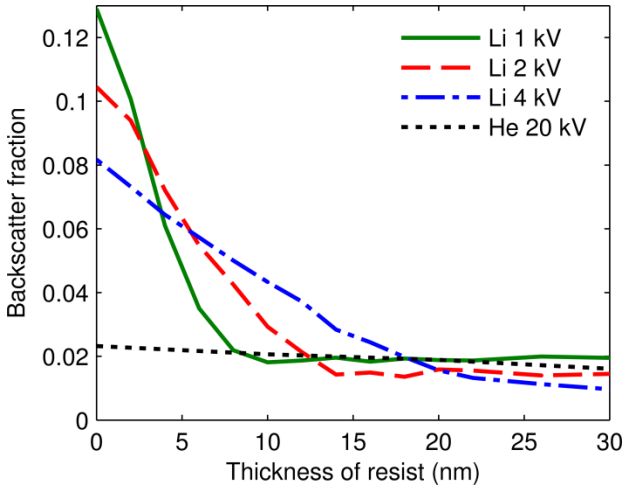

Figure 7. SRIM calculations of BSI yield from a simulated NIL target. Shown is the fraction of ions backscattered from a resist on a silicon target with varied resist thickness and ion beam energy. We compare to a 20 keV helium ion beam to demonstrate the expected result for BSI imaging in the HIM; the results for a high energy lithium ion beam are very similar.

NIL [30,31] is a promising nanofabrication technology to make sub-10 nm feature size devices. In this study, NXR-1025 thermal imprint resist [32] was patterned by a 4 μm pitch grating mold on a silicon substrate. Figure 6(a) shows a schematic of a grating test pattern after the imprint and mold release. As usual with this technique, a thin layer of residual resist remains in the spaces between the grating lines. For our sample, the resist lines were about 200 nm thick and the thin residual layer of resist between the lines had a thickness of about 30 nm. Oxygen plasma etching was then used to remove the bottom residual resist and expose the printed area on the substrate [Fig. 6(b)]. It is of critical importance for a NIL process to stop etching as soon as possible after the residual layer is removed to prevent over-etching of the printed pattern.

By taking lithium ion images at increasing etch times, the residual layer removal is observed as a stark change in contrast when the relatively high atomic number silicon substrate becomes visible to the ion beam, compared to the low atomic number organic resist [Fig. 6(c) and (d)]. Before and during etching, the contrast in the images is solely from topography, with the valleys of the grating appearing slightly dimmer than the peaks. After etching, there is elemental contrast between the exposed silicon in the valleys (bright) and the resist on the peaks (dark).

The uniquely low energy of the lithium ions is necessary to see this contrast change. The backscattering probability from the mostly carbon resist is generally very small and a high energy beam easily passes through the residual resist layer. But as the ions enter the silicon substrate, the backscatter yield becomes comparatively large and the large majority of the ions backscattered from the silicon layer will again pass through the resist layer on their way to the detector. Imaging with a high energy beam would effectively just image the silicon substrate, unless the resist layer is thick enough to stop the primary beam before it reaches the substrate, or stop the ions backscattered from the substrate before they escape the surface.

To demonstrate this quantitatively, we performed SRIM calculations for a simulated NIL target and the results are shown in Fig. 7. The target consists of a silicon substrate covered by a

resist layer of variable thickness. For each value of thickness, we recorded the fraction of backscattered ions. The yield matches that of pure silicon at zero thickness, and transitions to that of pure resist as the thickness approaches the range of the ion beam in the target. For a 1 keV beam, the length scale for this transition is about 5 nm, but for a 20 keV beam, there is almost no change in signal even with 30 nm of resist. This variation in backscatter yield explains the contrast in our images between the imprinted (0 nm to 30 nm thick) and un-imprinted (200 nm thick) lines.

Imaging the progress during etching is generally a challenging problem in NIL. Cross-sectional SEM is frequently used to measure the residual layer thickness and monitor the etching progress, but that requires coating with a conductive layer and typically destroys the sample, which is not practical in real NIL process control. Our technique provides imaging with clear contrast between the etched and unetched samples, providing a fast, non-destructive, albeit qualitative measure of the residual layer thickness. Alternative techniques may also be able to provide non-destructive imaging of this process, and we have made some preliminary measurements. For example, high quality images of the insulating uncoated samples can be taken by an environmental SEM or by a HIM (in iSE mode) using an electron flood gun for charge neutralization. But the difference in SE yield between a bare silicon substrate and one covered by a few nm layer of resist will be small compared to the large contrast in the backscattered lithium images. Also, variations in the amount of charge neutralization needed, as a function of resist thickness, may complicate a quantitative analysis. Backscattered electron detection from a very low energy electron beam of < 1 keV is an ideal candidate to provide elemental contrast with a surface sensitivity similar to 2 keV lithium ions, but we have had difficulty with electron beam damage to the resist when using large beam currents in this configuration. Careful choice of beam current and detector is needed to avoid this damage. A detailed comparison of these techniques is beyond the scope of this work.

5. SUMMARY

In summary, we have presented the capabilities and advantages of a low energy scanning ion microscope. We have obtained useful composition information from images based on the contrast in the yield of backscattered ions, and discussed the possibilities for unambiguous element identification. We have shown that backscattered lithium ion images provide non-destructive residual layer etching control in NIL fabrication, an accomplishment not easily achieved with existing instruments. We expect there to be many similar applications where our combination of good surface sensitivity, elemental contrast and high resolution imaging can provide an improvement on existing technologies. We also expect this to be the first of a wide variety of applications for the emerging technology of cold atom ion sources.

ACKNOWLEDGEMENTS

We thank Andras Vladar and Kate Klein for many useful discussions and for providing helium ion imaging of the NIL samples. We thank John Henry Scott for his assistance with the element standard measurements. We thank Glenn Holland, Alan Band, and Dave Rutter for their assistance designing and installing the microchannel plate detector system. Finally, we thank Brenton Knuffman and Adam Steele for their work during the early phases of this project. KAT acknowledges support under the Cooperative Research Agreement between the University of

Maryland and the National Institute of Standards and Technology Center for Nanoscale Science and Technology, Award 70NANB10H193, through the University of Maryland.

REFERENCES

[1] A.V. Steele, B. Knuffman, J.J. McClelland, J. Orloff, Focused chromium ion beam, J. Vac. Sci. Technol. B. 28 (2010) C6F1.

[2] B.J. Claessens, M.P. Reijnders, G. Taban, O.J. Luiten, E.J.D. Vredenbregt, Cold electron and ion beams generated from trapped atoms, Physics of Plasmas. 14 (2007) 093101.

[3] N. Debernardi, R.W.L. van Vliembergen, W.J. Engelen, K.H.M. Hermans, M.P. Reijnders, S.B. van der Geer, et al., Optimization of the current extracted from an ultracold ion source, New Journal of Physics. 14 (2012) 083011.

[4] J.L. Hanssen, S.B. Hill, J. Orloff, J.J. McClelland, Magneto-Optical-Trap-Based, High Brightness Ion Source for Use as a Nanoscale Probe, Nano Letters. 8 (2008) 2844–2850.

[5] B. Knuffman, A.V. Steele, J. Orloff, J.J. McClelland, Nanoscale focused ion beam from laser-cooled lithium atoms, New J. Phys. 13 (2011) 103035.

[6] B. Knuffman, A.V. Steele, J.J. McClelland, Cold atomic beam ion source for focused ion beam applications, J. Appl. Phys. 114 (2013) 044303–044303–7.

[7] A.J. McCulloch, D.V. Sheludko, S.D. Saliba, S.C. Bell, M. Junker, K.A. Nugent, et al., Arbitrarily shaped high-coherence electron bunches from cold atoms, Nature Physics. 7 (2011) 785–788.

[8] A.J. McCulloch, D.V. Sheludko, M. Junker, R.E. Scholten, High-coherence picosecond electron bunches from cold atoms, Nature Communications. 4 (2013) 1692.

[9] W.J. Engelen, M.A. van der Heijden, D.J. Bakker, E.J.D. Vredenbregt, O.J. Luiten, High-coherence electron bunches produced by femtosecond photoionization, Nat Commun. 4 (2013) 1693.

[10] J. Orloff, L.W. Swanson, M.W. Utlaut, High resolution focused ion beams: FIB and its applications: The physics of liquid metal ion sources and ion optics and their application to focused ion beam technology, Springer, 2003.

[11] B.W. Ward, J.A. Notte, N.P. Economou, Helium ion microscope: A new tool for nanoscale microscopy and metrology, J. Vac. Sci. Technol. B. 24 (2006) 2871–2874.

[12] H.H. Brongersma, M. Draxler, M. de Ridder, P. Bauer, Surface composition analysis by low-energy ion scattering, Surface Science Reports. 62 (2007) 63–109.

[13] T. Grehl, E. Niehuis, H.H. Brongersma, Surface Microanalysis by Low-Energy Ion Scattering, Microscopy Today. 19 (2011) 34–38.

[14] V.A. Esaulov, Low Energy Ion Scattering and Recoiling Spectroscopy in Surface Science, in: Surface Science Techniques, Springer, 2013: pp. 423–460.

[15] L. Kime, A. Fioretti, Y. Bruneau, N. Porfido, F. Fuso, M. Viteau, et al., High-flux monochromatic ion and electron beams based on laser-cooled atoms, Phys. Rev. A. 88 (2013) 033424.

[16] A.V. Steele, B. Knuffman, J.J. McClelland, Inter-ion coulomb interactions in a magneto-optical trap ion source, J. Appl. Phys. 109 (2011) 104308.

[17] J. Orloff, Fundamental limits to imaging resolution for focused ion beams, Journal of Vacuum Science & Technology B: Microelectronics and Nanometer Structures. 14 (1996) 3759.

[18] L. Scipioni, C.A. Sanford, J. Notte, B. Thompson, S. McVey, Understanding imaging modes in the helium ion microscope, J. Vac. Sci. Technol. B. 27 (2009) 3250–3255.
[19] R. Ramachandra, B. Griffin, D. Joy, A model of secondary electron imaging in the helium ion scanning microscope, Ultramicroscopy. 109 (2009) 748–757.
[20] M.T. Postek, A. Vladár, C. Archie, B. Ming, Review of current progress in nanometrology with the helium ion microscope, Meas. Sci. Technol. 22 (2011) 024004.
[21] D.C. Joy, B.J. Griffin, Is Microanalysis Possible in the Helium Ion Microscope?, Microscopy and Microanalysis. 17 (2011) 643–649.
[22] J. Ziegler, J. Biersack, M. Ziegler, SRIM—The Stopping and Range of Ions in Matter (SRIM Co., 2008), www.srim.org.
[23] G. Hlawacek, I. Ahmad, M.A. Smithers, E.S. Kooij, To see or not to see: Imaging surfactant coated nano-particles using HIM and SEM, Ultramicroscopy. 135 (2013) 89–94.
[24] S. Kostinski, N. Yao, Rutherford backscattering oscillation in scanning helium-ion microscopy, Journal of Applied Physics. 109 (2011) 064311–064311–7.
[25] S. Sijbrandij, B. Thompson, J. Notte, B.W. Ward, N.P. Economou, Elemental analysis with the helium ion microscope, J. Vac. Sci. Technol. B. 26 (2008) 2103–2106.
[26] S. Sijbrandij, J. Notte, L. Scipioni, C. Huynh, C. Sanford, Analysis and metrology with a focused helium ion beam, J. Vac. Sci. Technol. B. 28 (2010) 73–77.
[27] E. Taglauer, W. Englert, W. Heiland, D.P. Jackson, Scattering of Low-Energy Ions from Clean Surfaces: Comparison of Alkali- and Rare-Gas-Ion Scattering, Phys. Rev. Lett. 45 (1980) 740–743.
[28] M. Draxler, R. Gruber, H.H. Brongersma, P. Bauer, Velocity Scaling of Ion Neutralization in Low Energy Ion Scattering, Phys. Rev. Lett. 89 (2002) 263201.
[29] J. Druce, N. Simrick, T. Ishihara, J. Kilner, "Imaging" LEIS of micro-patterned solid oxide fuel cell electrodes, Nucl. Instrum. Meth. B. (2014), doi:10.1016/j.nimb.2014.02.074.
[30] S.Y. Chou, P.R. Krauss, P.J. Renstrom, Nanoimprint lithography, J. Vac. Sci. Technol. B. 14 (1996) 4129–4133.
[31] L.J. Guo, Nanoimprint Lithography: Methods and Material Requirements, Advanced Materials. 19 (2007) 495–513.
[32] Certain commercial product or equipment is described in this paper in order to specify adequately the experimental procedure. In no case does such identification imply recommendation or endorsement by the National Institute of Standards and Technology, nor does it imply that it is necessarily the best available for the purpose.